Soft Matter

Accepted Manuscript

ROYAL SOCIETY OF CHEMISTRY

www.rsc.org/softmatter

Controlling the Localization of Nanoparticles in Assemblies of Amphiphilic Diblock Copolymers

Shiying Ma[a,b], Dongliang Qi[a], Mengying Xiao[a], Rong Wang[*,a]

[a] Key Laboratory of High Performance Polymer Materials and Technology of Ministry of Education, Department of Polymer Science and Engineering, State Key Laboratory of Coordination Chemistry, School of Chemistry and Chemical Engineering, Nanjing National Laboratory of Microstructures, Nanjing University, Nanjing 210093, China

[b] College of Chemistry and Chemical Engineering, Taishan University, Taian 271021, China

We performed dissipative particle dynamics (DPD) approach to study the self-assembly of AB diblock copolymer tethered nanoparticles (P) in dilute solution. Different morphological aggregates, including spherical micelles, vesicles, disk-like micelles and rod-like micelles, were found by varying the interaction between block copolymer and nanoparticle. Most importantly, the nanoparticles can selectively localize in the different domains within the aggregates. When the repulsive interaction between block copolymer and nanoparticle a_{PA} = a_{PB} = 25, the nanoparticles evenly distributed within the spherical micelles. While a_{PA} or a_{PB} increases, the nanoparticles gradually aggregate and separate from copolymers and then localize in the central portion of vesicular wall or disk-like and rod-like micelles. The degree of stretching of tethered copolymer chain gradually grows with the increase of a_{PA} or a_{PB}. While the degree of stretching of solvophobic block B decreases when the morphologies change from sphere to disk-like micelle and further to rod-like micelle..This work illustrates that tuning the miscibility of copolymer and nanoparticle could be used to project the selective localization of nanoparticles within the aggregates self-assembled by diblock copolymer tethered nanoparticle in dilute solution.

1 Introduction

Assemblies containing block copolymers and nanoparticles have significant potential applications in biotechnology,biomedicine, catalysis, optics, electrics, etc, because they combine the desirable properties of nanoparticles and copolymers.[1-4] Many strategies have been employed for fabricating multifunctional nanostructures with tailored properties, such as direct incorporation of nanoparticles into the block copolymer

*Correspondence should be addressed. E-mail: wangrong@nju.edu.cn

matrix[5-7], using chemical coordination with organo-metallic compounds[8] or self-assembly of nanoparticles and copolymers in solution[9-14]. Self-assembly of block copolymers with nanoparticles in solution provides a powerful bottom-up method for constructing materials with desirable properties due to the possibility to fabricate nanostructures in a fast, simple, parallel and flexible manner. Furthermore, the self-assembly of amphiphilic nanoparticles with surface modified by copolymer chains has been extensively investigated in recent years, which provided an opportunity to achieve selective localization of nanoparticle in different domains of the copolymer aggregates or even in different parts of the same region of the aggregates. Lin et al[14] achieved organization of both polymeric and particulate entities through self-assembly without the use of external fields. Researchers can fabricate the nanostructural materials with hierarchical order using this simple and general route. Nikolic et al[15] investigated the self-assembly of the amphiphilic nanoparticles consisting of brush-like hydrophilic PEO chains and hydrophobic CdSe/CdS nanoparticles. They found the amphiphilic nanoparticles can self-assemble into spherical, cylindrical, and vesicular structures in dilute solution, which is driven by the surface density of the bound polymer chains. Li et al[16] reported the encapsulation of nanoparticles within the core of wormlike micelles through directed supramolecular assembly. They found that inter-particle spacing and micellar morphologies can be tailored by varying the nanoparticles or polymer brush content. Park and co-workers[17, 18] reported that the CdSe QDs and copolymers (PAA-*b*-PS) cooperatively self-assemble a novel structure in solution, which consists of an inner polymer core, an outer polymer shell, and the QDs spontaneously accumulated at the interface between the core and the shell. They found that the interaction between nanoparticle and block copolymer can dramatically affect the morphologies of block copolymer aggregates. However, these experimental researches were performed by controlling the morphologies of aggregates through varying the copolymer composition, the common solvent, the copolymer concentration, among other. Seldom research focuses on the effect of the interaction between nanoparticle and block copolymer on the selective localization of nanoparticles.[17, 18]

The theoretical simulation approaches, including molecular dynamics (MD), Brownian dynamics (BD)[19], Monte Carlo (MC)[20], dissipative particle dynamics (DPD)[21, 22], self-consistent field theory (SCFT)[23-27], etc, provide valuable microscopic insights and complement the deficiency of experimental studies on the self-assemble of polymer tethered nanoparticles.[28, 29] Glotzer and coworkers[30-35] used Brownian Dynamics simulation to systematically investigate the effect of the shape of building blocks, the nanoparticle polydispersity, etc, on the self-assembly of polymer tethered nanoparticles. Jayaraman and coworkers[20, 36-41] have shown the effect of the particle diameter, grafted chains length, monomer sequence, and grafting density on self-assembly behaviors in dense solution and melts of homopolymer or copolymer grafted nanoparticles using Polymer Reference Interaction

Site Model (PRISM) theory and Monte Carlo simulation. Recently, they have focused on the copolymer nanoparticle composition and interactions on phase behavior in both concentrated and dilute systems.[42, 43] Akcora et al.[44] have studied the effect of both polymer length and grafting density on the structure self-assembled by spherical polymer-grafted nanoparticle using simulation and experimental approaches. Zhu et al[23] studied the ordered nanostructures self-assembled from diblock copolymer tethered nanoparticle in bulk employed the combined self-consistent field theory (SCFT) and density functional theory (DFT). They found that the compatibility between nanoparticle and block copolymer dramatically influence the ordered nanostructure. But the important factor of the interaction between nanoparticle and block copolymer has been seldom studied in the dilute solution both in experiments and simulations. And there are many questions remaining unanswered. For example, how do nanoparticle-copolymer interactions affect the overall self-assembly of nanoparticle-grafted copolymer? How do nanoparticle-copolymer interactions affect the localization of nanoparticle in the aggregates?

In this paper, we employ dissipative particle dynamics (DPD) approach to study the self-assembly of diblock copolymer tethered nanoparticle in dilute solution, especially the localization of nanoparticles. We observe that while the alternating the interaction parameters produces different morphological aggregates, including spherical micelles, vesicles, disk-like micelles and rod-like micelles. Furthermore, we find that the nanoparticles can selectively localize in the different domains within the spherical micelles and vesicles. The paper is organized as follows. In Section 2 we provide details of the simulation methods and model. In Section 3 we present the results showing the effect of varying the interaction parameters between nanoparticle and copolymer on the morphologies of aggregates, the localization of nanoparticle within the aggregates. Section 4 concludes our study.

2 Method and Model

The dissipative particle dynamics (DPD) method, introduced by Hoogerbrugge and Koelman[45] in 1992, is a coarse-gained particle based mesoscopic simulation technique that allows the simulation of hydrodynamic behavior in much larger, complex systems, up to the microsecond range compared to the molecular dynamics (MD) simulations. In a DPD simulation, the coarse-gained DPD particles interact with each other via pair-wise interaction that contains conservative force $\boldsymbol{F}^{C}$, random force $\boldsymbol{F}^{R}$, and dissipative force $\boldsymbol{F}^{D}$. All the DPD particles obey Newton's equation of motion[46]:

$$\frac{d\vec{r}_i}{dt} = \vec{v}_i \quad , \quad \frac{d\vec{v}_i}{dt} = \frac{\vec{f}_i}{m_i} \tag{1}$$

where $\vec{r}_i$, $\vec{v}_i$, m_i and $\vec{f}_i$ denote the position, velocity, mass of the *i*th particle, and the acting force on it, respectively. The total force on the *i*th particle, $\boldsymbol{f}_i$, is the sum of all pair-wise interactions as

$$\vec{f}_i = \sum_{j \neq i} \left(\vec{F}_{ij}^{\mathrm{C}} + \vec{F}_{ij}^{\mathrm{D}} + \vec{F}_{ij}^{\mathrm{R}} \right) \tag{2}$$

The three pair-wise forces are given by

$$\vec{F}_{ij}^{\mathrm{C}} = a_{ij} \omega(r_{ij}) \hat{r}_{ij} \tag{3}$$

$$\vec{F}_{ij}^{\mathrm{D}} = -\gamma \omega^2(r_{ij})(\hat{r}_{ij} \bullet \vec{v}_{ij}) \hat{r}_{ij} \tag{4}$$

$$\vec{F}_{ij}^{\mathrm{R}} = \sigma \omega(r_{ij}) \theta_{ij} \hat{r}_{ij} \tag{5}$$

Where, a_{ij} is the repulsive interaction parameter between particle i and j, $\vec{r}_{ij} = \vec{r}_i - \vec{r}_j$, $r_{ij} = \left| \vec{r}_{ij} \right|$, $\hat{r}_{ij} = \vec{r}_{ij} / r_{ij}$, $\vec{v}_{ij} = \vec{v}_i - \vec{v}_j$. γ is the friction coefficient governing the magnitude of the dissipative force, σ is the noise amplitude that controls the intensity of the random force, and θ_{ij} is a randomly fluctuating variable with zero mean and unit variance. The combined effect of the dissipative and random force is that of a thermostat, leading to $\sigma^2 = 2\gamma k_{\mathrm{B}} T$.[46] The weight function $\omega(r_{ij})$ provides the range of interaction for DPD particle with a commonly used choice: $\omega(r_{ij}) = 1 - r_{ij} / r_{\mathrm{C}}$ for $r_{\mathrm{ij}} \leq r_{\mathrm{C}}$ and $\omega(r_{\mathrm{ij}}) = 0$ for $r_{\mathrm{ij}} > r_{\mathrm{C}}$, where r_{C} is the cutoff radius.[46]

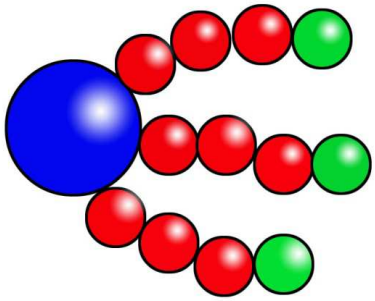

Figure 1. Model of three amphiphilic diblock copolymer tethered nanoparticle. The blue bead, red beads and green beads represent the nanoparticle (P), solvophobic block (B) and solvophilic block (A), respectively.

In this work, we focus on the model of amphiphilic diblock copolymer tethered nanoparticle $P_1(B_3A_1)_3$ as shown in Figure 1. The model is built by one nanoparticle bead and three diblock copolymers tethered on it. There are four different types of DPD particles, including nanoparticle beads (P), solvophobic beads (B), solvophilic beads (A), and solvent beads (S) in our simulation system. The concentration of block polymers with nanoparticles $P_1(B_3A_1)_3$ in the solution (φ) is defined as

$$\varphi = \frac{N_{pc} \times V_{pc} + N_n \times V_n}{N_{pc} \times V_{pc} + N_n \times V_n + N_s \times V_s} \tag{6}$$

where N_{pc}, N_n and N_s are the number of polymer chains beads, nanoparticle beads and solvent beads, respectively; V_{pc}, V_n and V_s are the volume of one bead of polymer chains, nanoparticle and solvent, respectively. The concentration of block polymers with nanoparticles (φ) is 0.10 unless otherwise stated in our simulation. The finitely extensible nonlinear elastic (FENE) potential is added between the consecutive particles to bind the connected beads of the diblock copolymer tethered nanoparticle.[47]

$$V_{FENE}(r_{ij}) = \begin{cases} -\frac{1}{2} k R_0^2 \ln\left[1 - \left(\frac{r_{ij}}{R_0}\right)^2\right] & r_{ij} < R_0 \\ \infty & r_{ij} \geq R_0 \end{cases} \tag{7}$$

We choose k = 30 and the finite extensibility of the FENE-spring $R_0 = 1.5 r_C$.[48] There is no extra angle forces between the tethers. Therefore, the three copolymer chains are free to move around the surface of the nanoparticle. The radius of a nanoparticle bead is 2 times of that of copolymer bead or solvent bead. Solvent beads are included explicitly in the simulation; however, they are not shown in the following figures for clarity.

On the basis of the model of the amphiphilic diblock copolymer tethered nanoparticle, we performed the dynamics of total 46875 DPD beads in a cubic box (25^3) under the periodic boundary conditions. The number density of all beads in the system is set to 3. In the present simulations, all the block copolymer and solvent beads are of the same mass as m = 1. The interaction cutoff radius for block copolymer and solvent particles is set to r_C = 1 as the unit of length, and energy scale $k_B T$ = 1. Here k_B is Boltzmann constant and T is the temperature. The time unit τ is defined as $\tau = \left(m r_C^2 / k_B T\right)^{1/2}$. Newton's equation of motion was integrated using modified velocity-Verlet algorithm with λ = 0.65. The DPD step was set as Δt = 0.03 to avoid divergence of the simulation and the amplitude of random noise is set as σ = 3.0. DPD simulation utilizes soft-repulsive potentials, the system studied are allowed to evolve much faster than the molecular dynamics. Therefore, a typical DPD simulation requires only about 10^5 steps to equilibrate.[46, 49] In our simulation, each simulation takes at least 1×10^6 steps and the 2×10^5 steps are for statistics. The conservative energy is found to reach steady state after about 1.5×10^3 DPD time. The variations of conservative energy of the copolymer tethered nanoparticles with time are given in ESI Figure S1. We have implemented the simulations with different initial random configurations and for various box sizes. The simulation results show that the morphology of aggregate at equilibrium is independent upon the initial conditions. The different size of boxes does not affect the formation of aggregations except the number of aggregates in the boxes

after equilibrium (ESI Table S1).[49]

The repulsive interaction parameters chosen are shown by a symmetric matrix

$$a_{ij} = \begin{pmatrix} & \text{P} & \text{B} & \text{A} & \text{S} \\ \text{P} & 25 & a_{\text{PB}} & a_{\text{PA}} & 150 \\ \text{B} & a_{\text{PB}} & 25 & 50 & 75 \\ \text{A} & a_{\text{PA}} & 50 & 25 & 25 \\ \text{S} & 150 & 75 & 25 & 25 \end{pmatrix} \quad (8)$$

Typically, the pair-wise repulsive interaction parameter between the same type of DPD particles is set as $a_{ii} = 25$ for density $\rho = 3$ to match the compressibility of water.[46] The interaction parameter between different particles i and j can be estimated by the relationship between the a_{ii} and Flory-Huggins interaction parameter χ_{ij} at $\rho = 3$ according to the relation[46]: $a_{ij} \approx a_{ii} + 3.27\chi_{ij}$ .The interaction parameters can be determined from the calculation of dimensionless compatibility. So the value of $a_{ij} \leq 25$ corresponds to $\chi_{ij} \leq 0$, which indicates that beads i and j are fairly compatible. As the incompatibility between i and j increases, a_{ij} rises from 25. The long polymer chains can be represented by short chains in DPD if the χ-parameter increases at the same time because χN can be used to describe the interaction of diblock copolymers.[46] Therefore, the long polymer chains on relatively small DPD chains with different interaction parameters can be actually simulated after applying these parameters.[46, 50] Here, since the nanoparticle and block B are solvophobic, we choose $a_{\text{PS}} = 150$ and $a_{\text{BS}} = 75$. Note that the repulsive interaction between the nanoparticle and solvent is stronger than that between solvophobic block B and solvent. The interaction parameter between solvophilic block A and solvent is set as $a_{\text{AS}} = 25$. The values of a_{PA} and a_{PB} are tunable in the simulation in order to examine the phase behavior of aggregates.

3 Results and discussion

A. Morphological diagram of the aggregates

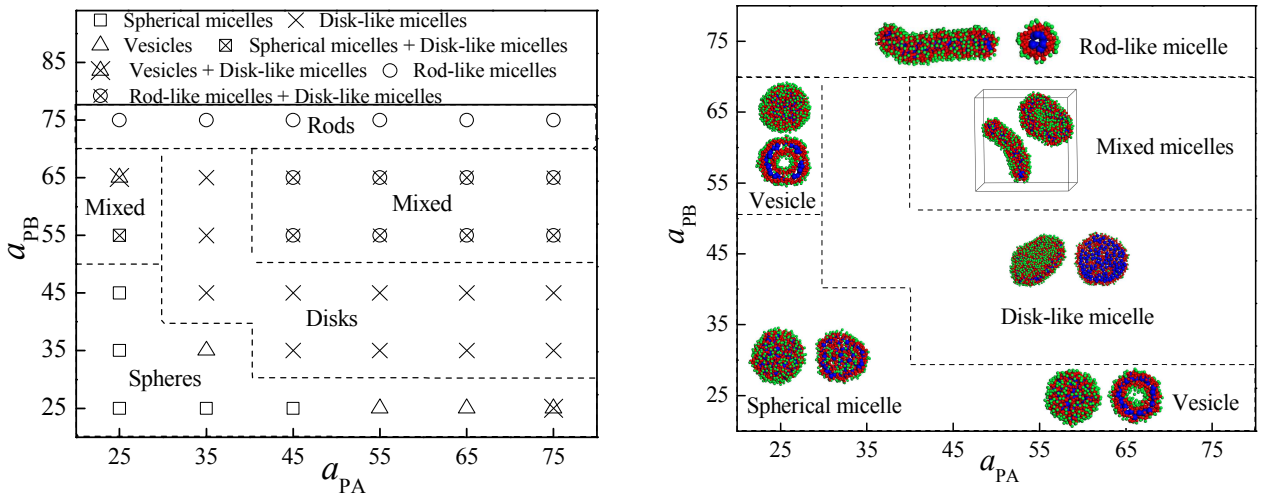

(a) (b)

Figure 2 (a) Morphological diagram of aggregates formed by diblock copolymer tethered nanoparticle in term of interaction parameters a_{PA} and a_{PB}. (b) Representative morphological snapshots are illustrated for various a_{PA} and a_{PB}. The green, red, and blue beads represent the block A, block B, and nanoparticle P, respectively.

In this section, we investigate the influence of the interaction between nanoparticle and block copolymer on the structures of the aggregates. By systematically changing the interaction parameters a_{PA} and a_{PB}, we examine the morphologies of aggregates and obtain the morphological diagram. Figure 2a shows the morphological diagram self-assembled by diblock copolymer tethered nanoparticle as a function of a_{PA} and a_{PB}. Four types of aggregates, (1) spherical micelles, (2) vesicles, (3) disk-like micelles and (4) rod-like micelles, are observed. The representative morphological snapshots are illustrated in Figure 2b. It is obvious that spherical micelles form with when a_{PA} = 25-65 and a_{PB} = 25 or a_{PA} = 25 and a_{PB} = 25-45, and rod-like micelles form with a_{PA} = 45-75 and a_{PB} = 55-75. Furthermore, the detailed regions of the disks and rods can be observed in Figure 2a. When a_{PB} = 35-45 and a_{PA} > 45, the disks become the dominating structure. Otherwise, rods form and become the final major structure in the range of a_{PB} = 55-75. There also exhibits mixed morphologies. This may be because the free energy levels of neighboring micellar morphologies are close to each other at equilibrium. In general, the interaction parameters between nanoparticle and block copolymer significantly affect the morphological structures of these aggregates. We also tried to explain the morphology transitions of micelles using the theories of Tanford[51-53] and Zhulina[54], but found that the certain observations do not fit either of the models. We will further investigate the morphology transitions of micelles based on the block copolymer model in the future studies.

B. Localization of nanoparticles within the aggregates

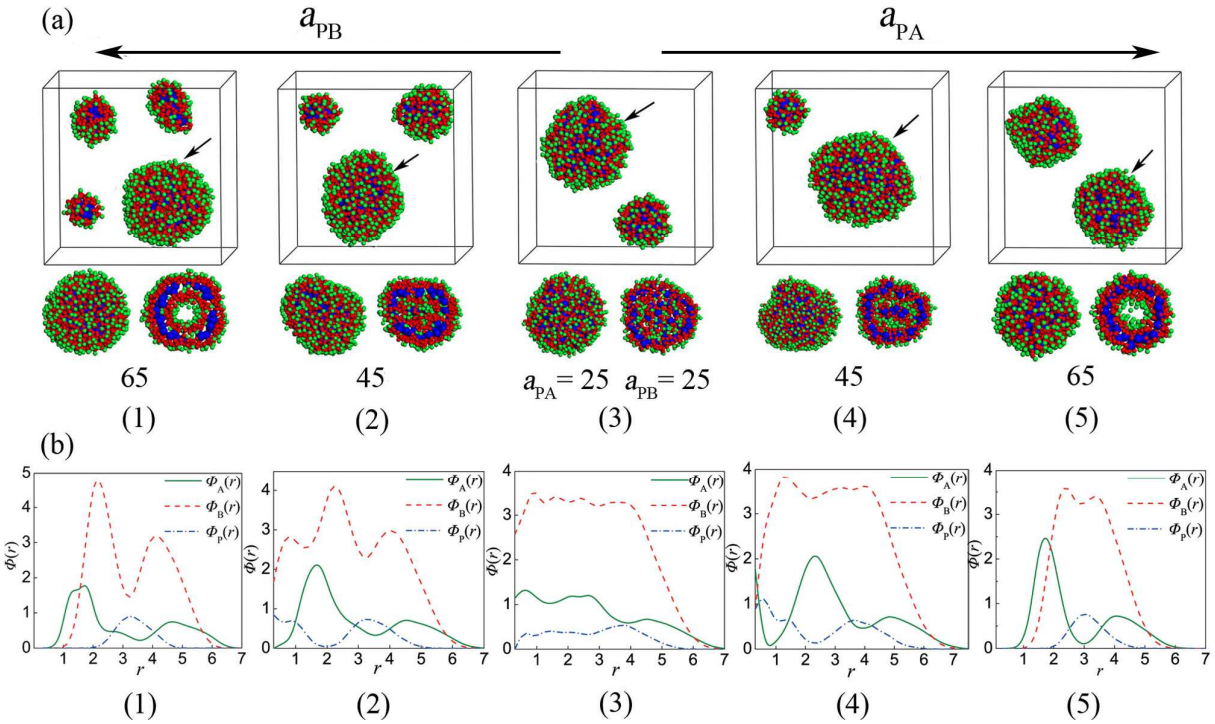

Figure 3 (a) Snapshots and cross-sectional slices of spherical micelles and vesicles with various a_{PA} and a_{PB}. The green, red, and blue colors represent A, B, and P beads, respectively. Solvent is omitted here for clarity. (b) Radial density function of the solvophilic block $\Phi_A(r)$ (green solid line), the solvophobic block $\Phi_B(r)$ (red dash line), and the nanoparticle $\Phi_P(r)$ (blue dash dot line) as a function of the distance r from the mass center of the aggregates corresponding to Figure 3a, respectively. Note that normalizations have been chosen such that $4\pi\int_0^R \phi_A(r)r^2 dr = N_A{}^{agg}$, the total number of solvophilic beads in the selected aggregate, $4\pi\int_0^R \phi_B(r)r^2 dr = N_B{}^{agg}$, the total number of solvophobic beads in the selected aggregate, and $4\pi\int_0^R \phi_P(r)r^2 dr = N_P{}^{agg}$, the total number of nanoparticles in the selected aggregate.

Selective localization of the nanoparticles within different domains of aggregates generated by the block copolymers may critically affect their resulting properties and potential applications. We examined the spherical micelles existed in the bottom and left part of diagram (Figure 2a) and investigated the distribution of nanoparticles in the aggregates as well as vesicles self-assembled by diblock copolymer tethered nanoparticle. Figure 3a shows the various distributions of nanoparticles in the spherical micelles and vesicles with different interaction parameter between nanoparticle and block copolymer. Figure 3b shows the radial density function of the solvophilic block A, solvophobic block B, and nanoparticle P as a function of the distance r from the mass center of aggregates

corresponding to Figure 3a. The nanoparticles uniformly localize in the micelle as $a_{PA} = a_{PB} = 25$ because of the compatibility between the nanoparticle and block copolymer (Figure 3a3 and 3b3). With the increase of a_{PB}, the incompatibility between nanoparticle and block B gradually increases, resulting in the segregation of nanoparticles and block B within the micelles (Figure 3a2 and 3b2). As a_{PB} further increases to 65, the nanoparticles locate in the central portion of the vesicle wall (Figure 3a1 and 3b1). This is not surprising. As a_{PB} increases, due to the increase of the repulsive interactions between nanoparticle and block B, the copolymer molecules stretch more to form nanoparticle P and block B segregated layers within micelles in order to reduce the contacts of them. Note that when a_{PB} increasing, the blocks B gradually move away from the nanoparticles, which results in block B separating from nanoparticles and lying in the vicinity of the nanoparticles due to the connection between block B and nanoparticles. Accordingly, blocks A move to the inner and outer layers of the micelles along with the blocks B (Figure 3b1 and 3b2). Similarly, as a_{PA} increasing, only the blocks A gradually move to the inner and outer of the aggregate, but blocks B move to the center of the aggregate (Figure 3a4 and 3b4). The nanoparticles and blocks B mix together in the micellar core, and blocks A locate in the micellar corona because the blocks A are far from the nanoparticles as well as their solvophilicity (Figure 3a5 and 3b5). Vesicles can be also observed in the range of a_{PA} = 55-75, the nanoparticles also locate in the wall of vesicles. However, the nanoparticles just selectively arrange in the vesicle membrane rather than in the obviously segmented central portion of the vesicle wall, which is because of the compatibility between the solvophobic nanoparticles and B-segments (Figure 3a5 and 3b5). Our simulation results are consistent with the experimental results. Both Eisenberg's group[55] and Park's group[12, 56] reported these interesting structures that nanoparticles are selectively located in the vesicle walls, as shown in Figure 3a1 or 3a5.

The copolymer chain conformations in micellar aggregates are important since they critically affect the formation and morphology of micelles. The block copolymers have relative flexible chain formation, which results in a large entropic contribution to the overall free energy during the micelle formation.[57] Therefore, the interplay between enthalpic and entropic contributions generates versatile morphologies for block copolymer micelles, associating with either stretching or compressing polymer chains to achieve free energy minimum.[58, 59] To better explain the results in Figure 3. We investigated the conformations of copolymer chains in micellar aggregates at equilibrium. In this work, we just investigate the variety of the degree of stretching of copolymer chain and solvophobic block B. The effect of them on the morphology transitions would be discussed in the future work. The end-to-end distances of the tethered copolymer chains and the solvophobic block B can be used to show the stretching of them. In our simulation systems, the end-to-end distance of the copolymer chain or solvophobic block B is shown in Figure 4.

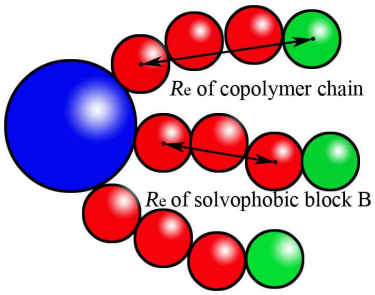

Figure 4 Illustration of end-to-end distance of copolymer chain and solvophobic block B.

The degree of stretching of tethered copolymer chain or solvophobic block B (S_c) is defined by[57, 60]

$$S_c = \left(\frac{\langle R_e^2 \rangle}{\langle R_{e0}^2 \rangle} \right)^{\frac{1}{2}} \quad (9)$$

Where R_e^2 is the mean square of the end-to-end distance of tethered copolymer chain or solvophobic block B in the aggregates in the simulation system. R_{e0}^2 is the mean square of the end-to-end distance of the tethered copolymer chain or solvophobic block B in the unperturbed state. We obtain the R_{e0}^2 through simulating the model copolymer in a good solvent, that is, the interaction parameters a_{ij} between the solvent and other species are all set to 25 and calculate the mean square of the end-to-end distance of the tethered copolymer chain or solvophobic block B.

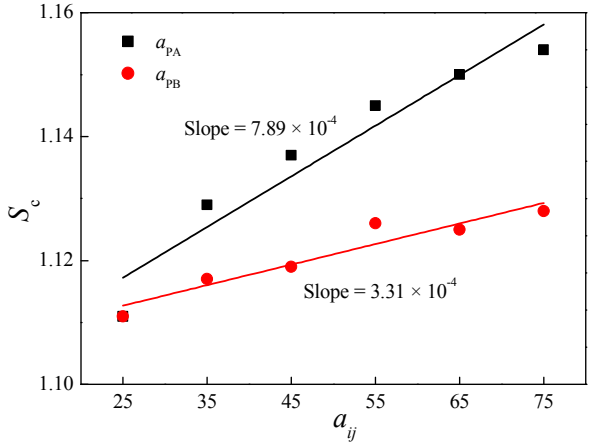

Figure 5 Average degree of stretching of the tethered copolymer chains as a function of a_{PA} as fixed a_{PB} = 25 (squares), and a_{PB} as fixed a_{PA} = 25 (spheres) at equilibrium.

Figure 5 shows the average degree of stretching of the tethered copolymer chains as a function of a_{PA} or a_{PB}. The quantified $<R_e^2>$ and S_c with various a_{PA} or a_{PB} are given in ESI Table S2 and S3. From Figure 5 and the data in

ESI Table S2 and S3, we can see that the copolymer chains grow more stretching with the increase of a_{PA} or a_{PB}. Furthermore, we found that the variation of a_{PA} more greatly affects the stretching of copolymer chains than that of a_{PB} from the slope of fitting lines (Figure 5), that is, the copolymer chains have a greater extension degree with the increase of a_{PA} than a_{PB}. Because the repulsive interaction between the nanoparticle and block A increase with increasing a_{PA} (Figure 5), and blocks A locate in the end of the chain. As a result, the extension of the copolymer chain would be more stretched. However, blocks B directly tether to the nanoparticle, the increase of a_{PB} mainly affect the stretching of the hydrophobic blocks B rather than the whole copolymer chains.

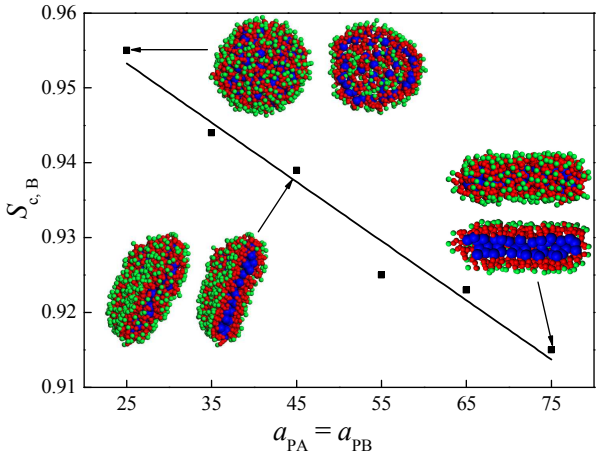

Figure 6 Degree of stretching of solvophobic block B in three representative aggregates with the increase of a_{PB} = a_{PA}. The green, red, and blue colors represent A, B, P beads, respectively. Solvent is omitted here for clarity.

Figure 6 shows the degree of stretching of solvophobic block B with various a_{PA} and a_{PB} in three representative aggregates. The quantified $<R_e^2>$ and S_c with various a_{PA} or a_{PB} are given in ESI Table S4. It is clear that the degree of stretching of block B decreases with the increase of a_{PA} and a_{PB}. This indicates that the blocks B are gradually compressed with the increase of a_{PA} and a_{PB}. Note that we found that the degree of stretching of solvophobic block B decreases as the morphologies change from sphere to rod-like micelle. This is consistent with the experimental findings by Zhang et al..[58] They found that the degrees of stretching of PS chains are decreased when the morphology transforms from spherical micelles to rod-like micelles with the decrease of PAA block length. The decrease of the degree of stretching accompanying the morphological transitions must be related to the geometric shapes of aggregates. Furthermore, we inquired into the localization of nanoparticles in the disk-like and rod-like micelles. It is interesting that the solvophobic nanoparticles all localize in the central portion of the disk-like and rod-like micelles (Figure 6). This may be because that a_{PB} is large enough to ensure that the solvophobic blocks B and the nanoparticles well segregate. Mai et al[61] have utilized the co-self-assembly of gold nanoparticles (AuNPs)

grafted with polystyrene$_{270}$-*block*-poly(acrylicacid)$_{15}$ (PS_{270}-*b*-PAA_{15}) and PS_{190}-*b*-PAA_{20} diblock copolymer to form the rods or micelles in solution. They can control the AuNPs into the central portion of block copolymer rods and micelles through this simply approach. Our model mimics the gold nanoparticles (AuNPs) grafted with PS_{270}-*b*-PAA_{15} and the similar aggregated structure, such as rod-like micelles, is observed in our simulation.

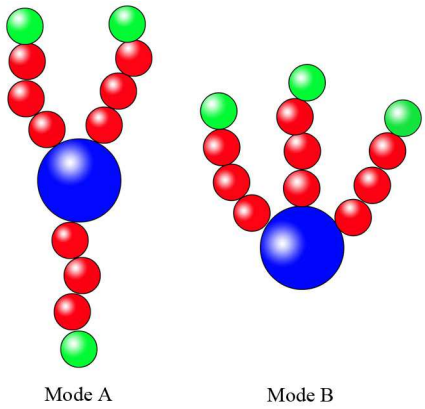

Figure 7 Illustration of the two packing modes of the tethered three copolymer chains.

Subsequently, we investigated the packing mode of the tethered copolymer chains. In this work, we just analyze the number fraction of different modes to present that the modes of the copolymer chains in different morphological aggregates seem to influence morphology transitions but the details of morphology transitions would be discussed in the future work. Because the tethered chains are free to move around the surface of the nanoparticle, the copolymer chains packing in aggregate have two modes. One is that the chains orient on the "top" and "bottom" of the nanoparticle (Mode A), another is that the three chains are all pushed to one side of the nanoparticle (Mode B), see Figure 7. We count the two different packing modes for spherical micelle, disk-like micelle, and rod-like micelle. The data of the number fraction of the two modes are given in ESI Table S5-8. The mode number fraction is about 0.393-0.432 in spherical micelles, and about 0.403-0.483 within vesicle membrane. However, in the disk-like and rod-like micelle, the copolymer chains are all pushed to one side of the nanoparticle (Mode B). This is caused by the increase of the repulsive interaction between the nanoparticle and copolymer chain. Therefore, the variation of interaction between the nanoparticle and copolymer chain would affect the chains packing mode.

4 Conclusions

We have employed dissipative particle dynamics (DPD) to study the self-assembly of diblock copolymer tethered nanoparticles in dilute solution. By varying the interaction parameters between the nanoparticle and the block

copolymer, the morphology and the phase diagram of the system of diblock copolymer tethered nanoparticles are obtained. The self-assembly of nanoparticles into different morphologies and the selective localization of nanoparticles within the aggregates can be tuned. The insight from this simulation work could guide experimentalists to project aggregates of functionalized particles through changing the miscibility of nanoparticle and copolymer chains.

The interaction parameters between the nanoparticle and the block copolymer greatly affect not only the morphology of aggregates but also the localization of nanoparticles within the aggregates. From the simulation results, we observed that alternating the interaction parameters produces different morphological aggregates, including spherical micelle, vesicle, disk-like micelle and rod-like micelle. Most importantly, the nanoparticles can selectively localize in the different domains within these spherical micelles and vesicles. When $a_{PA} = a_{PB} = 25$, the nanoparticles evenly distributed within the spherical micelles, while a_{PA} or/and a_{PB} increases, the nanoparticles gradually aggregate and separate from the block copolymer, then localize in the central portion of vesicular wall or the disk-like and rod-like micelles. We also found that the degree of stretching of tethered copolymer chain gradually grows with the increase of a_{PA} or a_{PB} in spherical micelles and vesicles. The degree of stretching of solvophobic block B decreases when the morphologies change from sphere to disk-like micelle and further to rod-like micelle..Generally, the present results shows the tailoring of the miscibility of copolymer and nanoparticle could be a new design knob to project the selective localization of nanoparticle within the aggregates self-assembled by diblock copolymer tethered nanoparticle in dilute solution. It should be noted that the basic assumption here is the block copolymer chains freely tethering on nanoparticles, which is in qualitative agreement with experiment. More general considerations should include grafting density, volume fraction of copolymers, as well as size of nanoparticle, which deserve further investigations.

Acknowledgement. This work was financially supported by the National Natural Science Foundation of China (grant nos. 21474051, 21074053 and 51133002), National Basic Research Program of China (grant no. 2010CB923303) and Program for Changjiang Scholars and Innovative Research Team in University (PCSIRT). The numerical calculations in this paper have been done on the IBM Blade cluster system in the High Performance Computing Center (HPCC) of Nanjing University.

References

1. J. F. Berret, N. Schonbeck, F. Gazeau, D. El Kharrat, O. Sandre, A. Vacher and M. Airiau, *J. Am. Chem. Soc.*,

2006, **128**, 1755-1761.

2. C. Sanson, O. Diou, J. Thevenot, E. Ibarboure, A. Soum, A. Brulet, S. Miraux, E. Thiaudiere, S. Tan, A. Brisson, V. Dupuis, O. Sandre and S. Lecommandoux, *ACS Nano*, 2011, **5**, 1122-1140.

3. X. H. Gao, Y. Y. Cui, R. M. Levenson, L. Chung and S. M. Nie, *Nat. Biotechnol.*, 2004, **22**, 969-976.

4. N. Nasongkla, E. Bey, J. M. Ren, H. Ai, C. Khemtong, J. S. Guthi, S. F. Chin, A. D. Sherry, D. A. Boothman and J. M. Gao, *Nano Lett.*, 2006, **6**, 2427-2430.

5. A. C. Balazs, T. Emrick and T. P. Russell, *Science*, 2006, **314**, 1107-1110.

6. S. Förster and M. Antonietti, *Adv. Mater.*, 1998, **10**, 195-217.

7. M. R. Bockstaller, R. A. Mickiewicz and E. L. Thomas, *Adv. Mater.*, 2005, **17**, 1331-1349.

8. R. B. Grubbs, *J. Polym. Sci., Part A: Polym. Chem.*, 2005, **43**, 4323-4336.

9. Y. Y. Mai and A. Eisenberg, *Acc. Chem. Res.*, 2012, **45**, 1657-1666.

10. A. Fahmi, T. Pietsch, C. Mendoza and N. Cheval, *Mater. Today*, 2009, **12**, 44-50.

11. Q. J. Luo, R. J. Hickey and S. J. Park, *ACS Macro Lett.*, 2013, **2**, 107-111.

12. R. J. Hickey, A. S. Haynes, J. M. Kikkawa and S. J. Park, *J. Am. Chem. Soc.*, 2011, **133**, 1517-1525.

13. B. L. Sanchez-Gaytan, S. Li, A. C. Kamps, R. J. Hickey, N. Clarke, M. Fryd, B. B. Wayland and S. J. Park, *J. Phys. Chem. C*, 2011, **115**, 7836-7842.

14. Y. Lin, A. Boker, J. He, K. Sill, H. Xiang, C. Abetz, X. Li, J. Wang, T. Emrick, S. Long, Q. Wang, A. Balazs and T. P. Russell, *Nature*, 2005, **434**, 55-59.

15. M. S. Nikolic, C. Olsson, A. Salcher, A. Kornowski, A. Rank, R. Schubert, A. Fromsdorf, H. Weller and S. Forster, *Angew. Chem., Int. Edit.*, 2009, **48**, 2752-2754.

16. W. K. Li, S. Q. Liu, R. H. Deng and J. T. Zhu, *Angew. Chem., Int. Edit.*, 2011, **50**, 5865-5868.

17. B. L. Sanchez-Gaytan, W. H. Cui, Y. J. Kim, M. A. Mendez-Polanco, T. V. Duncan, M. Fryd, B. B. Wayland and S. J. Park, *Angew. Chem., Int. Edit.*, 2007, **46**, 9235-9238.

18. A. C. Kamps, B. L. Sanchez-Gaytan, R. J. Hickey, N. Clarke, M. Fryd and S. Park, *Langmuir*, 2010, **26**, 14345-14350.

19. C. R. Iacovella, M. A. Horsch, Z. Zhang and S. C. Glotzer, *Langmuir*, 2005, **21**, 9488-9494.

20. T. B. Martin, A. Seifpour and A. Jayaraman, *Soft Matter*, 2011, **7**, 5952-5964.

21. S. Ma, M. Xiao and R. Wang, *Langmuir*, 2013, **29**, 16010-16017.

22. M. Y. Xiao, G. J. Xia, R. Wang and D. Q. Xie, *Soft Matter*, 2012, **8**, 7865-7874.

23. X. Zhu, L. Wang, J. Lin and L. Zhang, *ACS Nano*, 2010, **4**, 4979-4988.

24. Z. Liu, Z. Jiang, H. Yang, S. Bai, R. Wang and G. Xue, *Chinese J. Polym. Sci.*, 2013, **31**, 1491-1500.

25. R. Wang, Z. Jiang and G. Xue, *Polymer*, 2011, **52**, 2361-2365.

26. R. Wang, Y. Chen, J. Hu and G. Xue, *J. Chem. Phys.*, 2008, **129**, 44907.

27. R. Wang, Z. Jiang, Y. Chen and G. Xue, *J. Phys. Chem. B*, 2006, **110**, 22726-22731.

28. M. J. Hamer, B. V. S. Iyer, V. V. Yashin, T. Kowalewski, K. Matyjaszewski and A. C. Balazs, *Soft Matter*, 2014, **10**, 1374-1383.

29. Z. Posel, P. Posocco, M. Fermeglia, M. Lísal and S. Pricl, *Soft Matter*, 2013, **9**, 2936-2946.

30. C. L. Phillips and S. C. Glotzer, *J. Chem. Phys.*, 2012, **137**, 104901.

31. X. Zhang, Z. L. Zhang and S. C. Glotzer, *Nanotechnology*, 2007, **18**, 115706.

32. M. A. Horsch, Z. L. Zhang and S. C. Glotzer, *J. Chem. Phys.*, 2006, **125**, 184903.

33. S. C. Glotzer, M. A. Horsch, C. R. Iacovella, Z. L. Zhang, E. R. Chan and X. Zhang, *Curr. Opin. Colloid In.*, 2005, **10**, 287-295.

34. M. A. Horsch, Z. L. Zhang and S. C. Glotzer, *Phys. Rev. Lett.*, 2005, **95**, 56105.

35. Z. L. Zhang, M. A. Horsch, M. H. Lamm and S. C. Glotzer, *Nano Lett.*, 2003, **3**, 1341-1346.

36. A. Jayaraman and K. S. Schweizer, *Langmuir*, 2008, **24**, 11119-11130.

37. A. Jayaraman and K. S. Schweizer, *Macromolecules*, 2008, **41**, 9430-9438.

38. A. Jayaraman and K. S. Schweizer, *J. Chem. Phys.*, 2008, **128**, 164904.

39. A. Jayaraman and K. S. Schweizer, *Macromolecules*, 2009, **42**, 8423-8434.

40. N. Nair and A. Jayaraman, *Macromolecules*, 2010, **43**, 8251-8263.

41. T. B. Martin and A. Jayaraman, *Macromolecules*, 2013, **46**, 9144-9150.

42. C. E. Estridge and A. Jayaraman, *J. Chem. Phys.*, 2014, **140**, 144905.

43. H. S. Marsh, E. Jankowski and A. Jayaraman, *Macromolecules*, 2014, **47**, 2736-2747.

44. P. Akcora, H. Liu, S. K. Kumar, J. Moll, Y. Li, B. C. Benicewicz, L. S. Schadler, D. Acehan, A. Z. Panagiotopoulos, V. Pryamitsyn, V. Ganesan, J. Ilavsky, P. Thiyagarajan, R. H. Colby and J. F. Douglas, *Nature Materials*, 2009, **8**, 354-359.

45. P. J. Hoogerbrugge and J. M. V. A. Koelman, *Europhys. Lett.*, 1992, **19**, 155-160.

46. R. D. Groot and P. B. Warren, *J. Chem. Phys.*, 1997, **107**, 4423-4435.

47. M. Kroger and S. Hess, *Phys. Rev. Lett.*, 2000, **85**, 1128-1131.

48. M. Y. Xiao, J. N. Liu, J. X. Yang, R. Wang and D. Q. Xie, *Soft Matter*, 2013, **9**, 2434-2442.

49. H. Y. Chang, Y. L. Lin and Y. J. Sheng, *Macromolecules*, 2012, **45**, 4778-4789.

50. R. D. Groot and T. J. Madden, *J. Chem. Phys.*, 1998, **108**, 8713-8724.

51. C. Tanford, *Proc. Natl. Acad. Sci. U.S.A.*, 1979, **76**, 4175-4176.

52. C. Tanford, *J. Phys. Chem.*, 1974, **78**, 2469-2479.

53. C. Tanford, *Proc. Natl. Acad. Sci. U.S.A.*, 1974, **71**, 1811-1815.

54. E. B. Zhulina, M. Adam, I. LaRue, S. S. Sheiko and M. Rubinstein, *Macromolecules*, 2005, **38**, 5330-5351.

55. Y. Y. Mai and A. Eisenberg, *J. Am. Chem. Soc.*, 2010, **132**, 10078-10084.

56. R. J. Hickey, B. L. Sanchez-Gaytan, W. H. Cui, R. J. Composto, M. Fryd, B. B. Wayland and S. J. Park, *Small*, 2010, **6**, 48-51.

57. P. Bhargava, J. X. Zheng, P. Li, R. P. Quirk, F. W. Harris and S. Z. D. Cheng, *Macromolecules*, 2006, **39**, 4880-4888.

58. L. F. Zhang and A. Eisenberg, *J. Am. Chem. Soc.*, 1996, **118**, 3168-3181.

59. P. Bhargava, Y. Tu, J. X. Zheng, H. Xiong, R. P. Quirk and S. Z. D. Cheng, *J. Am. Chem. Soc.*, 2007, **129**, 1113-1121.

60. X. F. Yu, W. B. Zhang, K. Yue, X. P. Li, H. Liu, Y. Xin, C. L. Wang, C. Wesdemiotis and S. Cheng, *J. Am. Chem. Soc.*, 2012, **134**, 7780-7787.

61. Y. Y. Mai and A. Eisenberg, *Macromolecules*, 2011, **44**, 3179-3183.

Table of contents

Controlling the Localization of Nanoparticles in Assemblies of Amphiphilic Diblock Copolymers

Shiying Ma[a,b], Dongliang Qi[a], Mengying Xiao[a], Rong Wang[*,a]

[a] Key Laboratory of High Performance Polymer Materials and Technology of Ministry of Education, Department of Polymer Science and Engineering, State Key Laboratory of Coordination Chemistry, School of Chemistry and Chemical Engineering, Nanjing National Laboratory of Microstructures, Nanjing University, Nanjing 210093, China

[b] College of Chemistry and Chemical Engineering, Taishan University, Taian 271021, China

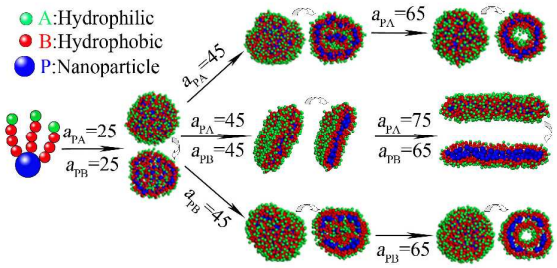

Localization of nanoparticles in assemblies of amphiphilic diblock copolymers can be controlled by varying the immiscibility of nanoparticles and copolymers.